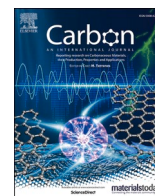




Contents lists available at ScienceDirect

Carbon

journal homepage: [www.elsevier.com/locate/carbon](http://www.elsevier.com/locate/carbon)

## Piezochromic luminescence of dicoronylene: Key for revealing hidden Raman modes at high pressure

Takeshi Nakagawa<sup>a,\*</sup>, Philip Dalladay-Simpson<sup>a</sup>, Kejun Bu<sup>a</sup>, Songhao Guo<sup>a</sup>, Martina Vrankić<sup>b</sup>, Dong Wang<sup>a</sup>, Raimundas Sereika<sup>a,c</sup>, Jianbo Zhang<sup>a</sup>, Caoshun Zhang<sup>a</sup>, Qingyang Hu<sup>a</sup>, Xujie Lü<sup>a</sup>, Yang Ding<sup>a,\*\*</sup>, Ho-kwang Mao<sup>a</sup>

<sup>a</sup> Center for High Pressure Science and Technology Advanced Research, 10 Xibeiwang East Road, Haidian District, Beijing, 100094, PR China

<sup>b</sup> Division of Materials Physics and Center of Excellence for Advanced Materials and Sensing Devices, Ruđer Bošković Institute, Bijenička 54, 10000, Zagreb, Croatia

<sup>c</sup> Vytautas Magnus University, K. Donelaičio Str. 58, LT-44248, Kaunas, Lithuania

### ARTICLE INFO

#### Keywords:

Polycyclic aromatic hydrocarbons  
Fluorescence  
Piezochromism  
Raman spectroscopy  
High pressure

### ABSTRACT

Molecular crystals of dicoronylene (C<sub>48</sub>H<sub>20</sub>), a member of very large polycyclic aromatic hydrocarbons (PAHs), exhibits strong red fluorescence under ambient conditions. This strong fluorescence induced by visible light excitation obscures entire Raman spectrum of dicoronylene. We employed in-situ high-pressure photoluminescence spectroscopy to observe a reversible piezochromic effect, in which the fluorescence exhibits a drastic red-shift with a rapid quenching of intensity. Above 4 GPa, under red-shifted and reduced fluorescence, hidden Raman modes are observed with 532 nm green laser up to 20 GPa. In this work, we show that the application of pressure can finely tune the fluorescence of dicoronylene, allowing the observation of the Raman spectrum with an appropriate laser wavelength and we discovered that dicoronylene has high chemical stability among PAH molecules with multiple aromatic rings.

### 1. Introduction

Polycyclic Aromatic Hydrocarbons (PAHs), carbon-rich organic molecular solids with high degree of  $\pi$ -conjugated structure, have attracted considerable interest for promising applications in functional devices such as organic photovoltaics, nanoelectronics, and semiconductors [1–5]. These unsaturated molecules consist of multiple fused aromatic rings, arranged in a herringbone structure and are characterized by a weak van der Waals interaction between them. Crystalline PAHs are characterized by their multiple resonance structures, which lead to the delocalization of valence electrons in the aromatic rings that can be easily excited, but their structure does not allow efficient vibrational relaxation, making them excellent fluorescent materials [6–8].

High pressure spectroscopic techniques provide a unique method to alter the effect of intermolecular interactions on the energy levels of molecules. Raman spectroscopy is one of the most powerful and informative techniques for monitoring physical changes and phase inhomogeneities in micrometer scale crystal domains in studies of PAHs [9,10]. Pressure-induced changes, such as, the energy of vibrational

excitations, phase transformations, chemical reactivity, and magnetic and electronic transitions can be effectively studied by in-situ Raman spectroscopy [11–13]. However, Raman measurements on luminescent PAH materials are often very challenging, because the strong fluorescence emission from the crystalline sample obscures the weak Raman scattering. In addition, some of the PAH molecules encounter pressure-induced fluorescence which obscures the Raman spectra with increasing pressure [14–18]. Under ambient conditions, the effect of fluorescence emission from PAH molecules can be checked and avoided by choosing an appropriate laser wavelength, i.e., to obtain a Raman spectrum in a lower energy region of the electromagnetic spectrum than the emitted fluorescence [19].

The pressure-induced emission changes in response to applied pressure are a phenomenon known as piezochromism, which is a direct consequence of the perturbation to the electronic band-gap energy of the electronic transition in luminescent materials. Such behaviour is often found in van der Waals materials, where the molecular packing is sensitive to and can be altered in response to external stimuli, resulting in significant changes in the chromaticity of their emission. Pressure can

\* Corresponding author.

\*\* Corresponding author.

E-mail addresses: [takeshi.nakagawa@hpstar.ac.cn](mailto:takeshi.nakagawa@hpstar.ac.cn) (T. Nakagawa), [yang.ding@hpstar.ac.cn](mailto:yang.ding@hpstar.ac.cn) (Y. Ding).

<https://doi.org/10.1016/j.carbon.2022.06.009>

Received 28 April 2022; Received in revised form 4 June 2022; Accepted 6 June 2022

Available online 9 June 2022

0008-6223/© 2022 Elsevier Ltd. All rights reserved.

induce different piezochromic behaviours in materials with different molecular structures via distinct piezochromisms, such as, the generation, enhancement, or quenching of fluorescence accompanied by a red/blue shift in its wavelength [20–25]. To better understanding of how fluorescence interferes with Raman spectroscopy of PAHs under high pressure, it is important to perform combined photoluminescence and Raman spectroscopic measurements.

In this work, we present the results of a systematic investigation on a single crystal dicoronylene ( $C_{48}H_{20}$ ), revealing the relationship between the pressure-dependent optical and vibrational properties. We combined Photoluminescence (PL), Raman, and Infrared (IR) spectroscopy and Synchrotron Powder X-ray Diffraction (SPXRD) measurements with Diamond Anvil Cell (DAC) techniques up to 20 GPa. At ambient conditions, dicoronylene shows strong red fluorescence emission when excited with visible lights, obscuring the entire Raman spectrum. When pressure is applied to dicoronylene, we observe a rapid decrease in the intensity of PL, accompanied by a large red-shift in the wavelength. Above 4 GPa, under reduced and red-shifted fluorescence, obscured Raman modes become visible and the number of observed Raman modes continue to increase up to 20 GPa, where over 60 Raman modes are identified. Our results demonstrate that by tuning the fluorescence of dicoronylene with the applied pressure, the obscured Raman modes can be observed by selecting an appropriate excitation laser. The observed Raman, IR spectra and SPXRD profiles show that dicoronylene has high chemical stability comparable to the smallest PAH molecules [26].

## 2. Experimental procedure

### 2.1. Sample preparation

The starting material of coronene ( $C_{24}H_{12}$ ) was purchased from TCI Chemicals (>98%) and purified by sublimation. Single crystal dicoronylene ( $C_{48}H_{20}$ ) was obtained by the vapor phase fusion reaction of coronene molecules. The sublimed coronene powder was placed in a long Pyrex tube and annealed for 5 h in a tube furnace (500 °C) with temperature gradient (−20 °C) to separate dicoronylene from pristine coronene. The furnace was cooled slowly (2 °C/h) to room temperature (RT) to obtain red needle-like crystals.

### 2.2. Single crystal X-ray diffraction at ambient conditions

Collection of single crystal X-ray diffraction data for dicoronylene was performed using a Bruker D8 VENTURE PHOTON II X-ray diffractometer with Photon 100 CMOS detector equipped with a Microfocus Incoated Ims 3.0, a Mo-target X-ray tube ( $\lambda = 0.71073 \text{ \AA}$ ), and a multilayer optic monochromator at RT. Data reduction and integration were performed with the Bruker software package SAINT. The structure was solved by SHELXT (version 2014/5) and refined by full-matrix least squares procedures using the Bruker SHELXL (version 2016/6) program [27]. The integration of the data using a monoclinic unit cell yielded a maximum  $\theta$  angle of 24.8 (0.85 Å resolution).

### 2.3. Diamond Anvil Cell (DAC)

Static high pressure was generated in a Mao-type symmetric DAC with 400  $\mu\text{m}$  culet-sized low-fluorescent anvils. A stainless steel gasket with 150  $\mu\text{m}$  hole was used for the sample compartment. Neon gas or silicon oil was loaded as a Pressure Transmitting Medium (PTM). Considering the inertness of PTM to the sample and the hydrostatic limits, inert gases, such as He and Ne are considered as the best PTM, where the non-hydrostaticity appears above 12 GPa and 15 GPa, respectively [28,29]. A small ruby ball was loaded with each crystal to determine the pressure by measuring the wavelength shift of the ruby  $R_1$  fluorescence line [30]. For optical spectroscopy and Raman spectroscopy measurements, choice of PTM does not have profound effect as the sample size and beam spot is very small, so the pressure deviation within

the sample chamber can be ignored.

### 2.4. Optical spectroscopy

Measurements of UV-vis absorption, fluorescence spectra, optical image, and photoluminescence images were performed with in-house developed Gora-UVN-FL (Ideaoptics, Shanghai) micro-region spectroscopy system. A single crystal dicoronylene ( $100 \times 40 \times 10 \mu\text{m}^3$ ) was loaded together with ruby ball into the sample chamber of a Mao-type symmetric DAC with 400  $\mu\text{m}$  culet-sized low-fluorescent anvils. Silicone oil was used as a PTM. Each pressure point was determined by the fitting pressure shift of the ruby fluorescence line.

### 2.5. Vibrational spectroscopy

Raman measurements were performed at ambient conditions with 532, 633, and 785 nm laser excitation on the MonoVista CRS + system (Spectroscopy & Imaging). A 300 grooves/mm grating was used in three measurements. The laser beam was focused on the sample with a 20  $\times$  objective lens, resulting in a laser spot of about 10  $\mu\text{m}$  diameter. Raman spectroscopy with 1064 nm laser excitation was performed using a Bruker IFS 66 instrument with a FRA 106 Raman module attachment and a  $\text{Nd}^{3+}$ /YAG laser. Laser power, exposure time, and number of accumulations were adjusted for each excitation laser used, and spectra were recorded over the wave number range of 15–3600  $\text{cm}^{-1}$ . Raman vibrational modes assignments were performed by first-principles simulations on the basis of density functional perturbation theory at the gamma center. The vibration vector matching each observed peak is traced and assigned to a specific motion types.

High-pressure Raman measurements were carried out with a custom-built highly focused Raman system, using 532 nm laser source. A single-crystal of dicoronylene (approximately  $50 \times 40 \times 10 \mu\text{m}^3$ ) was loaded along with a ruby ball into the sample chamber of a Mao-type symmetric DAC with 400  $\mu\text{m}$  culet-sized low-fluorescent anvils. Neon gas was used as a PTM. Measurements were imaged on a CCD, with a typical sample exposure of 0.01 s at 0.5 mW incident laser power.

High pressure Mid-IR spectra were obtained with Bruker VERTEX 70v IR spectrometer with HYPERION 2000 microscope in transmission mode in the range of 600–5000  $\text{cm}^{-1}$  in 2  $\text{cm}^{-1}$  per step. The spectrum of an empty DAC at ambient pressure was used as the background signal for all measurements. The sample chamber was filled with dicoronylene single crystals and compressed without PTM.

### 2.6. Synchrotron Powder X-ray diffraction (SPXRD) measurements

The in-situ high-pressure SPXRD experiment was carried out at Beamline 15U1 of Shanghai Synchrotron Radiation Facility (SSRF, P.R. China;  $\lambda = 0.6199 \text{ \AA}$ , beam size of  $4 \times 7 \text{ mm}^2$ ). Polycrystalline powder of dicoronylene was loaded along with a ruby ball into the sample chamber of a Mao-type symmetric DAC with 400  $\mu\text{m}$  culet-sized anvils. The sample chamber was fully packed with the sample powder and no PTM was used for this measurement. The SPXRD patterns were collected for 60 s at each pressure with a Mar-165 CCD detector and then integrated with Dioptas [31].

## 3. Results and discussion

### 3.1. Characterization of $C_{48}H_{20}$

Single-crystal XRD of dicoronylene under ambient conditions shows that it crystallizes in a monoclinic  $\beta$ -herringbone assembly with space group  $P2_1/c$ ,  $a = 10.3940(8) \text{ \AA}$ ,  $b = 3.8402(3) \text{ \AA}$ ,  $c = 31.990(3) \text{ \AA}$ ,  $\beta = 90.248(2)^\circ$ ,  $V = 1276.89(17) \text{ \AA}^3$ , which is consistent with previous result reported by Goddard (1995) [32]. Details of the crystal structure and the refined XRD data can be found in the Supplementary Information (SI-Fig. 1). The crystalline dicoronylene exhibits strong

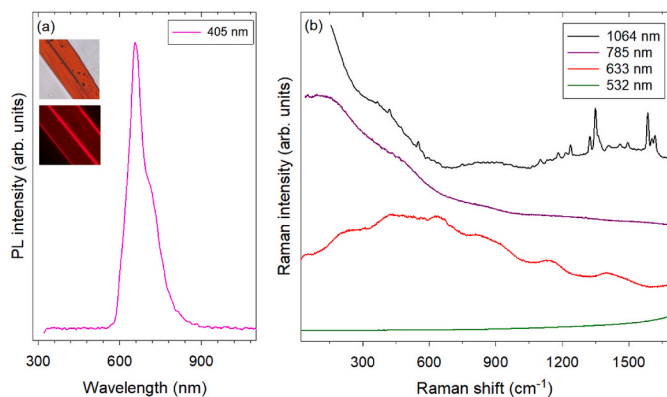


**Fig. 1.** (a) PL spectrum of a single-crystal  $C_{48}H_{20}$  at 405 nm laser. The inset: corresponding optical and PL image. (b) Raman spectra of  $C_{48}H_{20}$  at 1064, 785, 633, and 532 nm at ambient conditions. (A colour version of this figure can be viewed online.)

fluorescence with broad emission bands observed in the visible region between 570 and 870 nm, as shown by the photoluminescence micrographs demonstrating the bright red light emission from the sample at an excitation at 405 nm (Fig. 1a). According to the group theory, dicoronylene possesses 405 fundamental modes ( $102A_g + 101A_u + 102B_g + 100B_u$ ), where  $1A_u$  and  $2B_u$  modes are acoustic modes. Fig. 1b shows the Raman spectrum of dicoronylene at ambient conditions obtained with the four different laser excitation wavelengths, 1064, 785, 633, and 532 nm. The spectrum acquired using 785, 633, and 532 nm laser sources exhibits very high fluorescence that obscures all Raman bands. Of the 204 active Raman modes, 20 lines were observed when laser excitation at 1064 nm was used. The external modes in the low wavenumber range are obscured by the luminescent background and the C–H stretching modes between  $3100$  and  $3300\text{ cm}^{-1}$  were too weak at an excitation wavelength of 1064 nm. All internal Raman modes observed in our study and their assignments are listed in Table 1. The optical band-gap of dicoronylene at ambient conditions was estimated to be 2.2 eV by extrapolating the linear portion of the Kubelka-Munk function plots [33,34] of the UV–vis absorption spectra (SI-Fig. 2). This value is much smaller than that of most available PAHs, for example, benzene (6 eV), naphthalene (4.2 eV), phenanthrene (4.16 eV), triphenylene (3.95 eV), tetracene (2.54 eV), pyrene (3.03 eV), and coronene (3.1 eV) [35–38].

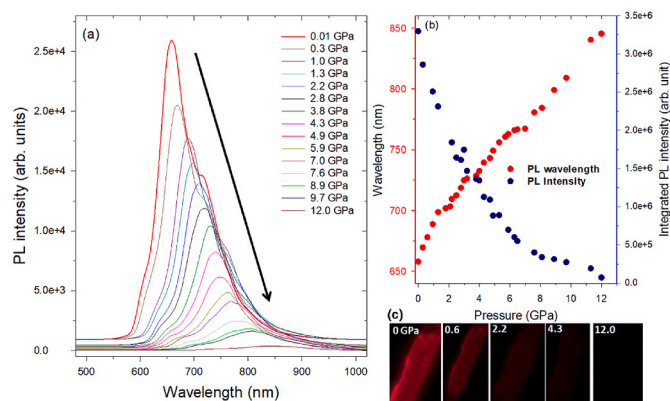
### 3.2. Pressure-dependent emission spectra

Fig. 2 shows the selected emission spectra of single-crystal  $C_{48}H_{20}$  under a pressure up to 12 GPa, which were obtained by a home-designed in-situ high-pressure optical properties measurement system using 405 nm excitation laser [39,40]. During the compression process, the peak maximum position of PL showed a continuous and significant red-shift from 658 nm (light red) to deep red and near-infrared (near-IR)

**Table 1**

Vibrational assignments of  $C_{48}H_{20}$  based on Raman spectra at 1064 nm.

Raman shift ( $\text{cm}^{-1}$ )	Mode Assignments
364	Ring squeezing
379	Ring bending
419	Ring squeezing
548	Ring stretching
1100	C–H wagging
1181	Ring wagging
1215	C–H wagging
1324–1617	C–C stretching
3042	C–H stretching
3278	C–H stretching



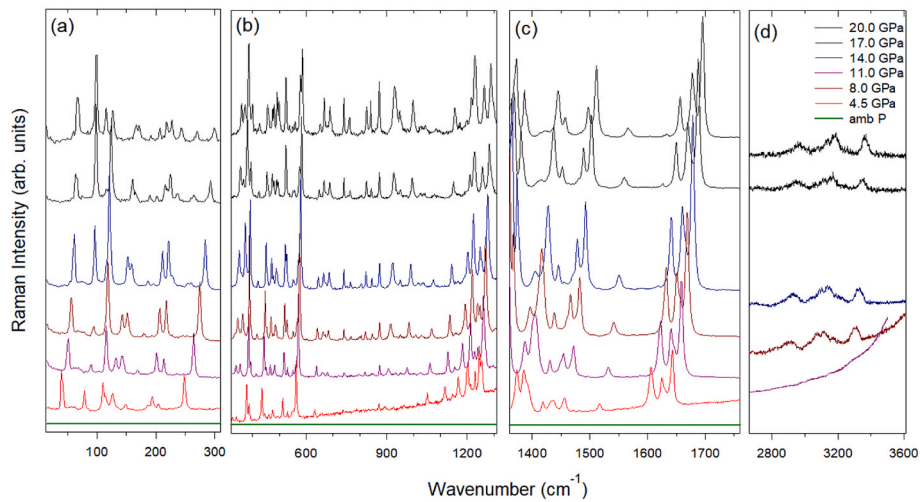
**Fig. 2.** (a) PL spectra of single-crystal  $C_{48}H_{20}$  in the pressure range of 0.01–12.0 GPa. The arrow indicates the change in PL intensity with increasing pressure. (b) Pressure-dependent emission wavelength (red, left axis) and integrated PL intensity (blue, right axis). (c) Fluorescence images of the single-crystal  $C_{48}H_{20}$  from 1 atm to 12.0 GPa. (A colour version of this figure can be viewed online.)

fluorescence (above 700 nm) and finally to 845 nm (dark red), a total shift of 187 nm ( $15.6\text{ nm/GPa}$ ) at 12 GPa. The pressure-dependent PL maximum position and integrated PL intensity are shown in Fig. 2b. The peak maximum position of PL undergoes red-shift with three slope changes at 2.2, 3.8, and 7.6 GPa, accompanying the change in crystal optical color from red to dark red, deep red, and then to black (SI-Fig. 3). The integrated intensity of PL drops rapidly and linearly in the pressure range below 8.0 GPa and decreases gradually up to 12.0 GPa. As can be seen in Fig. 2c, the PL intensity weakens continuously, with the integrated intensity of the PL peak at 12.0 GPa being only 2% of what was observed at ambient pressure and disappearing above 14 GPa. Such a change in crystal color and the attenuation of emission can be attributed to the reduction of intermolecular distances [41,42]. When the applied pressure was completely released from 14 GPa, the PL spectrum was restored to the original state, demonstrating the excellent reversibility of the process (SI-Fig. 4). The pressure-dependent piezochromic behaviour of dicoronylene can also be observed with a 532 nm excitation laser (SI-Fig. 5). The peak center showed continuous red-shift from 680 nm to 940 nm, a total shift of 260 nm ( $18.6\text{ nm/GPa}$ ), before disappearing completely at 15 GPa.

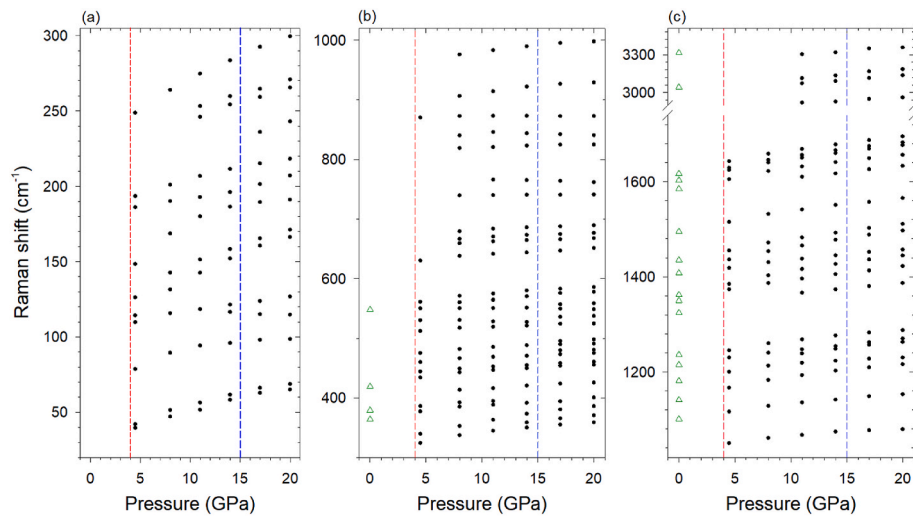
### 3.3. Pressure-dependent vibration spectroscopy

Fig. 3 shows the Raman spectra of the single-crystal  $C_{48}H_{20}$  at various pressures up to 20 GPa obtained during compression. The spectra were obtained by excitation with a 532 nm laser with a normal power density of  $0.5\text{ mW}/\mu\text{m}^2$  to avoid spectral changes due to radiation damage. At ambient conditions and at the initial compression below 2 GPa, all Raman modes are obscured by the strong fluorescence of dicoronylene. Above 2.5 GPa, only a few Raman modes become visible (3 Raman lines) as the peak maximum position of PL shifts to the near-IR region and the integrated PL intensity has been reduced by 50%. With further compression, the number of visible Raman modes and their intensity continue to increase. When the pressure was increased to 11.0 GPa, the integrated PL intensity was reduced by 94%, observable Raman modes increased to more than 60 Raman lines including C–H stretching modes above  $3000\text{ cm}^{-1}$ . Surprisingly, even at pressures well above 10 GPa, we did not observe any luminescence background formation interfering the Raman spectra, as was the case for other PAH molecules such as phenanthrene and pyrene (6.0 GPa) and naphthalene (15.0 GPa) [26].

The pressure-dependent peak frequencies of the observable Raman modes are shown in Fig. 4. The intermolecular modes are seen in the frequency range below  $200\text{ cm}^{-1}$ . The pressure shifts of these modes are



**Fig. 3.** Pressure-dependent Raman spectra of single-crystal  $C_{48}H_{20}$  recorded during compression with a 532 nm excitation laser. The spectra are divided into the low-frequency regions (a) and (b) and the high-frequency regions (c) and (d). After separation, the spectra were shifted vertically to minimize overlaps. In panel (d), the spectra for ambient pressure and 4.5 GPa are not included because the signal in this range exceeded the detection range. (A colour version of this figure can be viewed online.)



**Fig. 4.** Pressure-dependent Raman shift for single-crystal  $C_{48}H_{20}$  at RT obtained with a 532 nm excitation laser. Raman shifts are separated to three frequency ranges (a–c). The vertical dotted line at 4.0 GPa (red) and 15.0 GPa (blue) indicate the integrated intensity of PL reduced to 60% and to 0%, respectively. The green triangles are the Raman modes observed at ambient conditions with the 1064 nm excitation laser. (A colour version of this figure can be viewed online.)

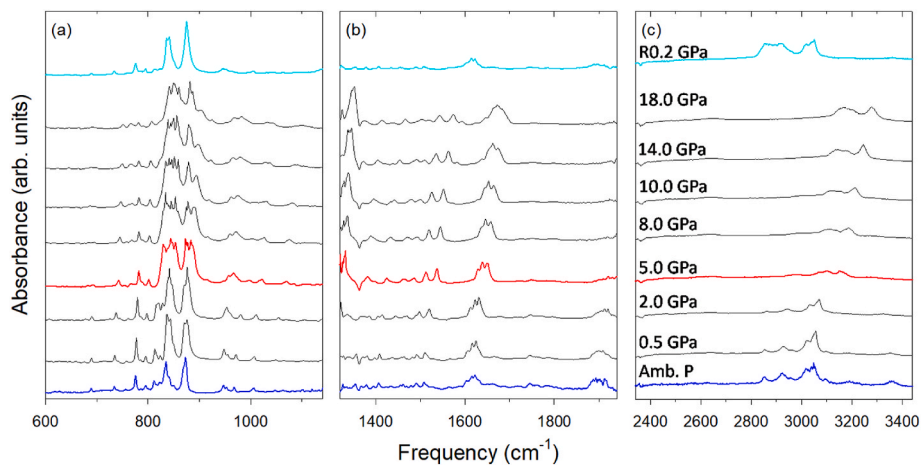


**Fig. 5.** Selected infrared spectra of  $C_{48}H_{20}$  up to 18.0 GPa and decompressed to 0.2 GPa at RT (a) mid-frequency region, (b) C–C stretching region and (c) C–H stretching region. (A colour version of this figure can be viewed online.)

sensitive to a decreases in intermolecular distances and shows rapid shifts in the low pressure range ( $4.9 \text{ cm}^{-1}/\text{GPa}$  up to 11 GPa), while smaller shifts, which are comparable to the intramolecular modes, are observed in the higher pressure range ( $1.0 \text{ cm}^{-1}/\text{GPa}$  above 11 GPa) (Fig. 4a). This indicates that the strength of intermolecular bonding changes with pressure, which coincides with the pressure at which fluorescence disappears. It is therefore, likely that fluorescence quenching in dicoronylene is related to the increased strength of intermolecular interactions and increased delocalization of  $\pi$ -electrons. The C–C modes are seen in the frequency range below  $1700 \text{ cm}^{-1}$ , shifting monotonically with increasing pressure at a rate of  $1 \text{ cm}^{-1}/\text{GPa}$ . They are generally much less affected by compression, but strongly affected by fluorescence. With red-shift and extinction of fluorescence, the number of observable Raman modes and the intensity of the modes increase rapidly above 8 GPa (Fig. 4b). The C–H stretching modes of dicoronylene in the Raman spectra are very weak compared to the other modes and become observable at above 11 GPa when the fluorescence has almost disappeared. The C–H stretches are also strongly affected by compression, where they exhibit a shift of  $7 \text{ cm}^{-1}/\text{GPa}$ . During compression above 4.5 GPa, the observed Raman modes shift positively without drastic changes up to 20.0 GPa.

Within the Raman spectra, it is not possible to discuss changes below 4.5 GPa because strong luminescence obscures the Raman modes. To investigate the effects of pressure on  $\text{C}_{48}\text{H}_{20}$  and their reversibility, we carried out IR measurements up to a maximum pressure of 18 GPa and decompressed to ambient conditions. Although, the use of IR spectroscopy on PAHs under pressure is still limited, IR is also a useful technique to identify the changes in molecular conformation. The advantage of IR over Raman spectroscopy is that its vibrational modes are extremely sensitive to changes in molecular conformation, but are not affected by red-shift or enhancement of fluorescence.

As shown in Fig. 5, the vibrational modes of IR exhibited linear blue shift with increasing pressure, indicating a shortening of intermolecular distances up to 18.0 GPa. At 5.0 GPa, changes were observed in the relative intensities of the C–H stretching modes at  $3150 \text{ cm}^{-1}$  and C–H out-of-plane (oop) modes ( $830$  and  $880 \text{ cm}^{-1}$ ). These intensity changes are the result of the compression-induced rearrangement of the molecules in terms of their distance and angles to fit the smaller unit cell, leading to an enhancement of the non-radiative vibrational motions. During compression, the molecules are packed denser in their herring-bone motif, leading to a gradual darkening of crystal colors, an enhancement of intermolecular interactions, and finally an attenuation of the fluorescence emission. This is consistent with the observed change in crystal color from light red to dark red and the appearance of Raman modes with decreasing PL intensity. After decompression from 18.0 GPa, an almost complete recovery of the original spectra features was observed at 0.2 GPa.

### 3.4. Pressure-dependent Synchrotron Powder X-ray diffraction

To confirm the effect of compression on the inter-molecular interaction, we carried out an in-situ high pressure SPXRD experiment at RT up to 20.2 GPa. Selected SPXRD profiles of the polycrystalline  $\text{C}_{48}\text{H}_{20}$  obtained at various pressure points are shown in Fig. 6. Examination of the SPXRD data shows that the reflection intensities are in excellent agreement with those single-crystal data at ambient pressure (SI-Fig. 6). Considering the cell parameters and space group extracted from the single-crystal data of  $\text{C}_{48}\text{H}_{20}$ , the unit cell metrics of polycrystalline data was evaluated using the LeBail algorithm at all pressures. All diffraction peaks shift continuously to higher angles consistent with contraction of the material, and there is no evidence of a structural phase transition over the investigated pressure range. The volume of the unit cell decreases rapidly during compression to 10.3 GPa, with the lattice parameters  $a$ ,  $b$ , and  $c$  reduced by 6%, 4.7%, and 3%, respectively and the overall volume of the unit cell decreased by 13% (SI-Fig. 7). A least-squares fit of the equation of state (EOS) with the third-order Birch-

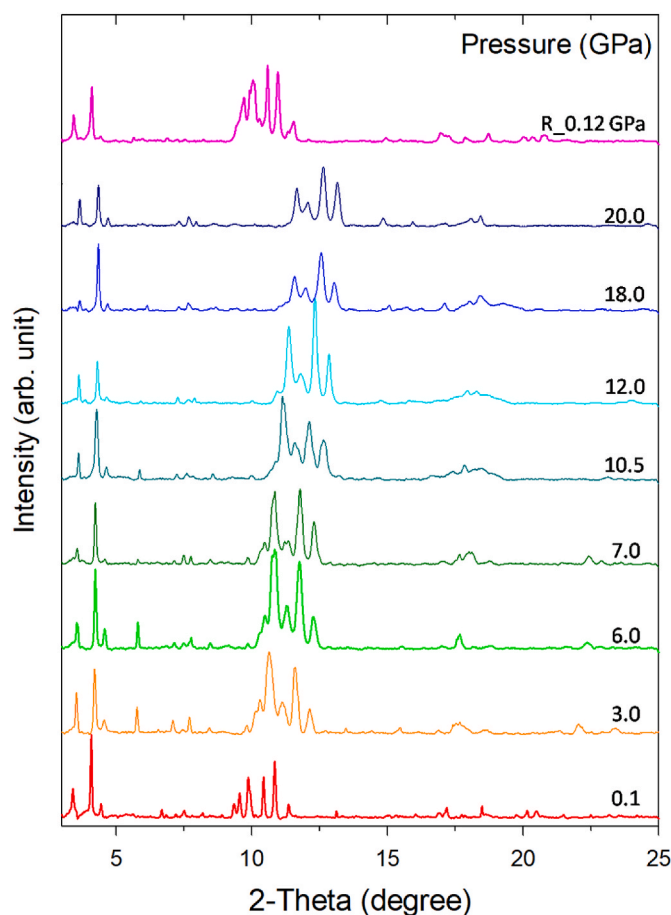


Fig. 6. Synchrotron Powder X-ray ( $\lambda = 0.6199 \text{ \AA}$ ) diffraction profile of  $\text{C}_{48}\text{H}_{20}$  obtained during compression from 0.05 to 20.0 GPa and during decompression to 0.1 GPa. (A colour version of this figure can be viewed online.)

Murnaghan EOS [43] was performed using EosFit 7 software [44], with the fit leading to the values of the isothermal bulk modulus,  $K_0 = 10.7$  (7) GPa and the pressure derivative  $K_0' = 42.5$  (4). It should be noted that the optical property of the sample changes to a dark red during compression above 5.0 GPa, but no change in crystal symmetry was observed up to 20.2 GPa, which is in excellent agreement with Raman and IR spectroscopy measurements. Although change in the crystal symmetry was not observed, unit cell volume evolution above 15 GPa maybe indicating possible phase transition. The high-pressure SPXRD data confirm that the change in crystal color and attenuation of fluorescence are due to the enhancement of the intermolecular interaction resulting from the rearrangement of the molecules.

From 20.2 GPa, the applied pressure was slowly released and SPXRD data were also collected with decreasing pressure down to 0.12 GPa. The displaced diffraction peaks show a continuous shift to lower angles and a return to the original position, which was accompanied by a recovery of the red color of the material.

### 3.5. Discussion

Compared to other probes, Raman spectroscopy has technical advantages that it can be performed for solids, liquids and gases, with the sample size can be as small as submicron level, and variety of laser wavelength can be employed to generate a Raman spectrum. However, at high pressure, considering the excitation efficiency, sample sensitivity, and spectrometer configuration, it is common to use visible laser excitation. Among the various techniques available to probe PAHs under high pressure, the challenges in using Raman spectroscopy is to extract

Raman signatures from broadband fluorescence emissions. Indeed, several recent Raman studies by different groups on various PAHs at moderately high pressures have difficulty in resolving the obtained Raman spectrum due to interference from luminescence [14–18]. On the other hand, the study of pressure-induced luminescence of these PAHs has rarely received sufficient attention.

The optical properties of PAHs largely depend on the size and geometry of the constituent molecules, with their optical absorption and emission behaviour showing characteristic fingerprint spectra for different molecules [45,46]. In addition, the applied hydrostatic pressure can modulate the molecular packing modes and conformation, with a different compressibility of PAHs leading to a characteristic relationship between their molecular structure and their physical and chemical properties [26,47,48]. In the case of dicoronylene, the estimated optical band-gap at ambient conditions is 2.2 eV, which allows the electronic transitions between the valence band and the conduction band using lasers with any wavelength in UV, visible, and IR ranges. The intensity of the resulting fluorescence is an order of magnitude higher than that of the Raman lines, and therefore obscures entire Raman modes under ambient conditions. At high pressure, interference is much less, as the PL shifts to the near-IR region. In the case of pyrene, one of the well-studied small PAH molecules, the estimated optical band-gap at ambient conditions is 3.64 eV [38]. A shorter wavelength laser (e.g. 320 nm) is required to excite the electron in the case of larger optical band-gap, and pyrene exhibits broad fluorescence emission band at 350–500 nm [35]. Therefore, the use of excitation wavelength of 633 nm can collect Raman spectra without having interference from the emission at ambient condition. It has been reported that the fluorescence of pyrene has continuous shift of PL peak maximum position to 582 nm with increasing hydrostatic pressure up to 10.2 GPa [49], which is consistent with the appearance of extensive luminescence above 5.0 GPa in the Raman spectra [15,26]. Thus, the pressure at which the luminescence interferes with Raman modes depends on the position of characteristic fluorescence band and the distinct piezochromic behaviour of the individual PAH molecules with different molecular structures.

#### 4. Conclusion

In summary, we performed optical and vibration spectroscopic study of dicoronylene under compression. We observed a strong red fluorescence of dicoronylene that rapidly shifts to the near-IR region and is suppressed with increasing pressure. Obscured Raman modes at ambient conditions were observed above 4.5 GPa as the red-shifted and suppressed fluorescence interfered much less with Raman scattering obtained with a green laser. The chemical stability of single-crystal dicoronylene was indicated by the number of vibrational modes observed at 20 GPa, making it one of the most stable PAH molecules composed of multiple rings. Analysis of high pressure IR and Raman results showed that there is no structural phase transition and chemical reaction below 20 GPa. The increase in C–H stretching and oop vibrational modes at 5 GPa indicates stronger intermolecular interactions, which are responsible for the change in crystal color and attenuated PL emission. The study of the piezochromic behaviour of dicoronylene was key to rediscovery of hidden Raman modes at high pressure, which provided valuable information about vibrational properties in response to the applied pressure. These combined optical vibrational spectroscopic measurements can also be used for other PAH molecules to find out how piezochromic behaviour can affect vibrational properties and how they can differ with different composition and arrangement of aromatic rings.

#### Notes

The authors declare no competing financial interest.

#### CRedit authorship contribution statement

**Takeshi Nakagawa:** Conceptualization, Investigation, Formal analysis, Writing – original draft. **Philip Dalladay-Simpson:** Investigation. **Kejun Bu:** Investigation. **Songhao Guo:** Investigation. **Martina Vrankić:** Formal analysis, Writing – review & editing. **Dong Wang:** Formal analysis. **Raimundas Sereika:** Formal analysis. **Jianbo Zhang:** Formal analysis. **Caoshun Zhang:** Formal analysis. **Qingyang Hu:** Formal analysis. **Xujie Lü:** Writing – review & editing. **Yang Ding:** Funding acquisition, Supervision, Writing – review & editing. **Hokwang Mao:** Funding acquisition, Supervision, Writing – review & editing.

#### Declaration of competing interest

The authors declare that they have no known competing financial interests or personal relationships that could have appeared to influence the work reported in this paper.

#### Acknowledgements

This work was financially supported by the National Key Research and Development Program of China (2018YFA0305703), the Science Challenge Project (No. TZ2016001), and the National Natural Science Foundation of China (NSFC: U1930401, 11874075, 42150101).

#### Appendix A. Supplementary data

Supplementary data to this article can be found online at <https://doi.org/10.1016/j.carbon.2022.06.009>.

#### References

- [1] S.R. Forrest, The path to ubiquitous and low-cost organic electronic appliances on plastic, *Nature* 428 (2004) 911–918, <https://doi.org/10.1038/nature02498>.
- [2] B. Fang, H. Zhou, I. Honma, Electrochemical Lithium doping of a pentacene molecule semiconductor, *Appl. Phys. Lett.* 86 (2005), 261909, <https://doi.org/10.1063/1.1954873>.
- [3] V. Podzorov, Organic single crystals: addressing the fundamentals of organic electronics, *MRS Bull.* 38 (2013) 15–25, <https://doi.org/10.1557/mrs.2012.306>.
- [4] S. Ahmad, Organic semiconductors for device applications: current trends and future prospects, *J. Polym. Eng. 34* (4) (2014) 279–338, <https://doi.org/10.1515/polyeng-2013-0267>.
- [5] J. Liu, H. Zhang, H. Dong, L. Meng, L. Jiang, L. Jiang, Y. Wang, J. Yu, Y. Sun, W. Hu, A.J. Heeger, High mobility emissive organic semiconductor, *Nat. Commun.* 6 (2015), 10032, <https://doi.org/10.1038/ncomms10032>.
- [6] J. Xiao, H. Yang, Z. Yin, J. Guo, F. Boey, H. Zhang, Q. Zhang, Preparation, characterization and photoswitching/light-emitting behaviours of coronene nanowires, *J. Mater. Chem.* 21 (2011) 1423–1427, <https://doi.org/10.1039/c0jm02350g>.
- [7] J.B. Birks, L.G. Christophorou, Excimer fluorescence of aromatic hydrocarbons in solution, *Nature* 194 (1962) 442–444, <https://doi.org/10.1038/194442a0>.
- [8] H. Nishimura, T. Yamaoka, K. Mizuno, M. Iemura, A. Matsui, Luminescence of free and self-trapped excitons in  $\alpha$ - and  $\beta$ -perylene crystals, *J. Phys. Soc. Japan* 53 (1984) 3999–4008, <https://doi.org/10.1143/JPSJ.53.3999>.
- [9] A. Brillante, I. Bilotti, R.G. Della Valle, E. Venuti, A. Girland, Probing polymorphs of organic semiconductors by lattice phonon Raman microscopy, *CrystEngComm* 10 (2008) 937–946, <https://doi.org/10.1039/b804317e>.
- [10] A.D. Chanyshev, K.D. Litasov, A.F. Shatskiy, Y. Furukawa, T. Yoshino, E. Ohtani, Oligomerization and carbonization of polycyclic aromatic hydrocarbons at high pressure and temperature, *Carbon* 84 (2015) 225–235, <https://doi.org/10.1016/j.carbon.2014.12.011>.
- [11] E. del Corro, M. Taravillo, J. González, V.G. Baonza, Raman characterization of carbon materials under non-hydrostatic conditions, *Carbon* 49 (2011) 973–979, <https://doi.org/10.1016/j.carbon.2010.09.064>.
- [12] A.F. Goncharov, Raman spectroscopy at high pressures, *Int. J. Spectrosc.* (2012), 617528, <https://doi.org/10.1155/2012/617528>.
- [13] V.A. Davydov, A.V. Rakhmanina, V. Agafonov, B. Narymbetov, J.-P. Boudou, H. Swarc, Conversion of polycyclic aromatic hydrocarbons to graphite and diamond at high pressures, *Carbon* 42 (2004) 261–269, <https://doi.org/10.1016/j.carbon.2003.10.026>.
- [14] L. Zhao, B.J. Baer, E.L. Chronister, High-pressure Raman study of anthracene, *J. Phys. Chem. A* 103 (1999) 1728–1733, <https://doi.org/10.1021/jp9838994>.
- [15] B. Sun, Z.A. Dreger, Y.M. Gupta, High-pressure effects in pyrene crystals: vibrational spectroscopy, *J. Phys. Chem. A* 112 (42) (2008) 10546–10551, <https://doi.org/10.1021/jp806382x>.

- [16] Q.-W. Huang, J. Zhang, A. Berlie, Z.-X. Qin, X.-M. Zhao, J. Zhang, et al., Structural and vibrational properties of phenanthrene under pressure, *J. Chem. Phys.* 139 (2013), 104302, <https://doi.org/10.1063/1.4820359>.
- [17] X.-M. Zhao, G.-H. Zhong, J. Zhang, Q.-W. Huang, A.F. Goncharov, H.-Q. Lin, X.-J. Chen, Combined experimental and computational study of high-pressure behavior of triphenylene, *Sci. Rep.* 6 (2016), 25600, <https://doi.org/10.1038/srep25600>.
- [18] X.-M. Zhao, J. Zhang, A. Berlie, Z.-X. Qin, Q.-W. Huang, S. Jiang, et al., Phase transformation and vibrational properties of coronene under pressure, *J. Chem. Phys.* 139 (2013), 144308, <https://doi.org/10.1063/1.4824384>.
- [19] A.J. Alajlat, H.G.M. Edwards, M.A. Elbagerma, I.J. Scowen, The effect of laser wavelength on the Raman Spectra of phenanthrene, chrysene, and tetracene: implications for extra-terrestrial detection of polyaromatic hydrocarbons, *Spectrochim. Acta, Part A* 76 (2010) 1–5, <https://doi.org/10.1016/j.saa.2010.01.009>.
- [20] Y. Dai, H. Liu, T. Geng, F. Ke, S. Niu, K. Wang, Y. Qi, B. Zou, B. Yang, W.L. Mao, Y. Lin, Pressure-induced excimer formation and fluorescence enhancement of an anthracene derivative, *J. Mater. Chem. C* 9 (2021) 934, <https://doi.org/10.1039/d0tc04677a>.
- [21] Y. Dong, B. Xu, J. Zhang, X. Tan, L. Wang, J. Chen, H. Lv, S. Wen, B. Li, L. Ye, B. Zou, W. Tian, Piezochromic luminescence based on the molecular aggregation of 9,10-bis((E)-2-(pyrid-2-yl)vinyl)anthracene, *Angew. Chem. Int. Ed.* 51 (2012) 10782–10785, <https://doi.org/10.1002/anie.201204660>.
- [22] H. Liu, Y. Gu, Y. Dai, K. Wang, S. Zhang, G. Chen, B. Zou, B. Yang, Pressure-induced blue-shifted and enhanced emission: a cooperative effect between aggregation-induced emission and energy-transfer suppression, *J. Am. Chem. Soc.* 142 (2020) 1153–1158, <https://doi.org/10.1021/jacs.9b11080>.
- [23] H. Liu, Y. Dai, Y. Gao, H. Gao, L. Yao, S. Zhang, Z. Xie, K. Wang, B. Zou, B. Yang, Y. Ma, Monodisperse  $\pi$ - $\pi$  stacking anthracene dimer under pressure: unique fluorescence behaviors and experimental determination of interplanar distance at excimer equilibrium geometry, *Adv. Opt. Mater.* 6 (2018), 1800085, <https://doi.org/10.1002/adom.201800085>.
- [24] T. Schillmoller, R. Herbst-Irmer, D. Stalke, Insights into excimer formation factors from detailed structural and photophysical studies in the solid-state, *Adv. Opt. Mater.* 9 (2021), 2001814, <https://doi.org/10.1002/adom.2020001814>.
- [25] H. Liu, Y. Shen, Y. Yan, C. Zhou, S. Zhang, B. Li, L. Ye, B. Yang, One stimulus in situ induces two sequential luminescence switchings in the same solvent-fuming process: anthracene excimer as the intermediate, *Adv. Funct. Mater.* (2019), 1901895, <https://doi.org/10.1002/adfm.201901895>.
- [26] E. O'Bannon, Q. Williams, Vibrational spectra of four polycyclic aromatic hydrocarbons under high pressure: implications for stabilities of PAHs during accretion, *Phys. Chem. Miner.* 43 (2016) 181–208, <https://doi.org/10.1007/s00269-015-0786-1>.
- [27] G.M. Sheldrick, Crystal structure refinement with shelxl, *Acta Crystallogr. A* 71 (2015) 3–8, <https://doi.org/10.1107/S2053229614024218>.
- [28] H.K. Mao, X.J. Chen, Y. Ding, B. Li, L. Wang, Solids, liquids, and gases under pressure, *Rev. Mod. Phys.* 90 (55) (2018), 015007, <https://doi.org/10.1103/RevModPhys.90.015007>.
- [29] S. Klotz, J.-C. Chervin, P. Munsch, G. Le Marchand, Hydrostatic limits of 11 pressure transmitting media, *J. Phys. D Appl. Phys.* 42 (7) (2009), 075413, <https://doi.org/10.1088/0022-3727/42/7/075413>.
- [30] H.K. Mao, J. Xu, P.M. Bell, Calibration of the ruby pressure gauge to 800 kbar under quasi-hydrostatic conditions, *J. Geophys. Res.* 91 (1986) 4673–4676, <https://doi.org/10.1029/JB091iB05p04673>.
- [31] C. Prescher, V.B. Prakapenka, DIOPTAS: a program for reduction of two-dimensional X-ray diffraction data and data exploration, *High Pres. Res.* 35 (3) (2015) 223–230, <https://doi.org/10.1080/08957959.2015.1059835>.
- [32] R. Goddard, M.W. Haanel, W.C. Herndon, C. Krüger, M. Zander, Crystallization of large planar polycyclic aromatic hydrocarbons: the molecular and crystal structures of hexabenzob[bc,ef,hi,kl,no,qr]coronene and benzo[1,2,3-bc:4,5,6-b'c']dicoronene, *J. Am. Chem. Soc.* 117 (1995) 30–41, <https://doi.org/10.1021/ja00106a004>.
- [33] P. Kubelka, F.A. Munk, Contribution to the optics of pigments, *Z. Technol. Phys.* 12 (1931) 593–599.
- [34] P. Makula, M. Pacia, W. Macyk, How to correctly determine the band gap energy of modified semiconductor photocatalysts based on UV-vis spectra, *J. Phys. Chem. Lett.* 9 (2018) 6814–6817, <https://doi.org/10.1021/acs.jpclett.8b02892>.
- [35] R. Rieger, K. Müllen, Forever young, Polycyclic aromatic hydrocarbons as model cases for structural and optical studies, *J. Phys. Org. Chem.* 23 (2010) 315–325, <https://doi.org/10.1002/poc.1644>.
- [36] J.C.S. Costa, R.J.S. Taveira, C.F.R.A.C. Lima, A. Mendes, L.M.N.B.F. Santos, Optical band gaps of organic semiconductor materials, *Opt. Mater.* 58 (2016) 51–60, <https://doi.org/10.1016/j.optmat.2016.03.041>.
- [37] A. Menon, J.A.H. Dreyer, J.W. Martin, J. Akroyd, J. Robertson, M. Kraft, Optical band gap of cross-linked, curved, and radical polyaromatic hydrocarbons, *Phys. Chem. Chem. Phys.* 21 (2019), <https://doi.org/10.1039/C9CP02363A>, 16240–1625.
- [38] J.C.S. Costa, R.M. Campos, L.M.S.S. Lima, M.A.V. Ribeiro da Silva, L.M.N.B.F. Santos, On the aromatic stabilization of fused polycyclic aromatic hydrocarbons, *J. Phys. Chem. A* 125 (2021) 3696–3709, <https://doi.org/10.1021/acs.jpca.1c01978>.
- [39] S. Guo, K. Bu, J. Li, Q. Hu, H. Luo, Y. He, Y. Wu, D. Zhang, Y. Zhao, W. Yang, M. G. Kanatzidis, X. Lü, Enhanced photocurrent of all-inorganic two-dimensional perovskite Cs<sub>2</sub>PbI<sub>2</sub>Cl<sub>2</sub> via pressure-regulated excitonic features, *J. Am. Chem. Soc.* 143 (2021) 2545–2551, <https://doi.org/10.1021/jacs.0c11730>.
- [40] X. Lü, C. Stoumpos, Q. Hu, X. Ma, D. Zhang, S. Guo, J. Hoffman, K. Bu, X. Guo, Y. WQang, C. Ji, H. Chen, H. Xu, Q. Jia, W. Yang, M.G. Kanatzidis, H.-K. Mao, Regulating off-centering distortion maximizes photoluminescence in halide perovskites, *Natl. Sci. Rev.* 8 (2021) nwa288, <https://doi.org/10.1093/nsr/nwaa288>.
- [41] W. Cai, R. Zhang, Y. Yao, S. Deemyad, Piezochromism and structural and electronic properties of benz[a]anthracene under pressure, *Phys. Chem. Chem. Phys.* 19 (2017) 6216–6223, <https://doi.org/10.1039/C6CP08171A>.
- [42] S. Fanetti, M. Citroni, L. Malavasi, G.A. Artioli, P. Postorino, R. Bini, High-pressure optical properties and chemical stability of picene, *J. Phys. Chem. C* 117 (2013) 5343–5351, <https://doi.org/10.1021/jp4006789>.
- [43] F.D. Murnaghan, The compressibility of media under extreme pressures, *Proc. Natl. Acad. Sci. U.S.A.* 30 (1944) 244–247, <https://doi.org/10.1073/pnas.30.9.244>.
- [44] J. Gonzalez-Platas, M. Alvaro, F. Nestola, R. Angel, EosFit7-GUI: a new graphical user interface for equation of state calculations, analyses and teaching, *J. Appl. Crystallogr.* 49 (2016) 1377–1382, <https://doi.org/10.1107/S1600576716008050>.
- [45] S. Feng, Y. Yang, L. Gao, K. Watanabe, T. Taniguchi, Z. Hu, J. Lu, Z. Ni, Tunable self-trapped excitons in 2D layered rubrene, *Appl. Phys. Lett.* 118 (2021), 253103, <https://doi.org/10.1063/5.0049942>.
- [46] N. Nijegorodov, R. Mabbs, W.S. Downey, Evolution of absorption, fluorescence, laser and chemical properties in the series of compounds perylene, benzo(ghi)perylene and coronene, *Spectrochim. Acta, Part A* 57 (2001) 2673–2685, [https://doi.org/10.1016/S1386-1425\(01\)00457-7](https://doi.org/10.1016/S1386-1425(01)00457-7).
- [47] M. Du, J. Dong, Y. Zhang, X. Yang, Z. Li, M. Wang, R. Liu, B. Liu, Q. Zhou, T. Wei, B. Liu, Vibrational properties and polymerization of coronulene under pressure, probed by Raman and infrared spectroscopies, *J. Phys. Chem. C* 123 (2019) 23674–23681, <https://doi.org/10.1021/acs.jpcc.9b03261>.
- [48] F. Capitani, M. Höppner, B. Joseph, L. Malavasi, G.A. Artioli, L. Baldassarre, A. Perucchi, M. Piccinini, S. Lupi, P. Dore, L. Boeri, P. Postorino, Combined experimental and computational study of the pressure dependence of the vibrational spectrum of solid picene C<sub>22</sub>H<sub>14</sub>, *Phys. Rev. B* 88 (2013), 144303, <https://doi.org/10.1103/PhysRevB.88.144303>.
- [49] A. Li, Y. Liu, C. Bi, W. Xu, Z. Ma, H. Cui, S. Xu, Pressure-dependent distinct luminescent evolutions of pyrene and TPA-Py single crystals, *Spectrochim. Acta, Part A* 237 (2020), 118390, <https://doi.org/10.1016/j.saa.2020.118390>.